Research Article | Vol. 12, No. 2 / 1 February 2021 / Biomedical Optics Express 893
Biomedical Optics EXPRESS

Anisotropic scattering characteristics of nanoparticles in different morphologies: improving the temperature uniformity of tumors during thermal therapy using forward scattering

QIN CHEN,[1,2] YATAO REN,[1,2,3] YANMEI YIN,[1] AND HONG QI[1,4]

[1]School of Energy Science and Engineering, Harbin Institute of Technology, Harbin 150001, China
[2]Faculty of Engineering, University of Nottingham, University Park, Nottingham NG7 2RD, UK
[3]renyt@hit.edu.cn
[4]qihong@hit.edu.cn

Abstract: Precise control of the thermal damage area is the key issue during thermal therapy, which can be achieved by manipulating the light propagation in biological tissue. In the present work, a method is proposed to increase the uniformity of the specific absorption rate (SAR) distribution in tumors during laser-induced thermal therapy, which is proved to be effective in reducing the thermal damage of healthy tissue. In addition, a better way of manipulating light propagation in biological tissue is explored. It is found that the anisotropic scattering characteristics of nanoparticles are strongly dependent on their shapes, sizes, orientations, and incident wavelengths, which will strongly affect the light propagation in nanoparticle embedded biological tissue. Therefore, to obtain a better outcome from photothermal therapy, the scattering properties of nanoparticles are very important factors that need to be taken into consideration, along with the absorption efficiency. Further investigation finds that nanoparticles that predominantly scatter to the forward direction are favorable in obtaining a larger penetration depth of light, which will improve the uniformity of SAR and temperature distributions. This paper is meaningful for the application of nanoparticle-assisted laser-induced thermal therapy.

1. Introduction

As an important alternative treatment for cancer, nanoparticle-assisted laser induced thermal therapy (LITT) has drawn much attention in recent years [1–4]. Most of the recent investigations are focused on, but not limited to, light and heat propagation in biological tissues embedded with nanoparticles [1,5], developing advanced nano-therapeutic agents [6–8], and new strategies for LITT [9–12]. Very recently, Alrahili et al. reported experimental and theoretical studies of the photothermal efficiency of gold nanoparticles in different sizes and morphologies, including nanospheres, nanorods, nanourchins, and nanosphere conjugates [13]. It was found that decorating a dye that absorbs 808 nm light can enhance the photothermal efficiency for nanospheres, which paves a new way for the development of possible new candidates for photothermal therapy. Despite the rapidly increasing research interests in this area, several remaining problems must be solved, among which the unwanted damage of healthy tissue is a non-negligible issue that must be settled in practice.

The most important purpose for introducing plasmonic nanoparticles to the process of LITT is to improve the selective heating of cancerous tissue [14–16]. However, the selective effect is only realized on a certain level. Specifically, for non-invasive cases, when the light is irradiated at the tissue surface, it needs to transfer through healthy tissue before reaching the targeted tumor. Even if one assumes that the superficial tissue is nearly transparent, which means the heat generation in healthy tissue can be neglected, light still attenuates rapidly after it reaches the interface between nanoparticle-embedded cancerous tissue and surrounding healthy tissue, which means that the

#415666 https://doi.org/10.1364/BOE.415666
Journal © 2021 Received 23 Nov 2020; revised 29 Dec 2020; accepted 8 Jan 2021; published 15 Jan 2021

Biomedical Optics EXPRESS

light induced heat source is basically distributed near the tumor surface. Therefore, to induce thermal damage of deeper cancerous tissue, the surrounding healthy tissue will be inevitably heated due to heat diffusion. The accurate prediction and manipulation of light propagation in biological tissue embedded with nanoparticles are the key issues to confront in solving the above-mentioned problem.

To accurately predict light propagation and absorption in biological tissue, the anisotropic scattering of biological tissue and nanoparticles should be taken into consideration. However, with extensive growing interest in the study of the absorption properties of plasmonic nanoparticles [16,17], their scattering effects, especially their scattering directivity are often neglected. In other words, to simulate light transportation in biological tissue embedded with plasmonic nanoparticles, the scattering contribution of nanoparticles is often overlooked or simply treated as isotropic scattering. The anisotropic scattering properties of high-refractive-index dielectric nanoparticles are extensively investigated due to their low dissipative losses and thermal heating [18–23]. However, regarding plasmonic nanoparticles, researchers care more about their localized heat generation rates, which is to say, the absorption property of plasmonic nanoparticles seems more important than their scattering property. For applications that involve both heat and optical propagation, the scattering properties of plasmonic nanoparticles also play an extremely important role. The most representative example is the above-mentioned nanoparticle-assisted LITT, in which accurate prediction of light transportation is of equal importance or even more important than heat generation and diffusion.

Therefore, the light scattering of plasmonic nanoparticles is worth further investigation. In the studies of absorption properties of plasmonic nanoparticles, wavelengths corresponding to the localized surface plasmon resonance (LSPR) have always been paid special attention [8,24], due to its high photothermal conversion efficiency, which means that in LITT the wavelength corresponding to the LSPR of nanoparticles is the first choice to enhance the light absorption in targeted area. However, it is not the only optical characteristic that one must take into consideration. In the present work, we mainly focused on the impact of anisotropic scattering of nanoparticles on the temperature field of biological tissue during photothermal therapy, in which the particles concentration is kept as constant. The influence of light-to-heat conversion efficiency and concentration of nanoparticles have been investigated in our previous work and other relative works [1,25–27], which will not be discussed here.

2. Theoretical approaches

The scattering and absorption properties of isolated nanoparticles with different geometries and materials are calculated by the discrete dipole approximation (DDA). The basic principle of DDA is to discretize nanoparticles into a cubic array of virtual N-point dipoles [28]. Then, the scattering field of the entire particle can be approximated as the summation of all the dipoles, which means that it can be applied to obtain the optical properties of arbitrarily shaped targets. The polarization of the ith dipole can be expressed as $\mathbf{P}_j = \alpha_j \mathbf{E}_j$, where α_j is the polarizability of the jth dipole and $\mathbf{E}_j$ is the electric field in position $\mathbf{r}_j$, which can be obtained by [28]:

$$\mathbf{E}_j = \mathbf{E}_j^{\mathrm{inc}} - \sum_{k \neq j} \mathbf{A}_{jk} \mathbf{P}_k \tag{1}$$

where $\mathbf{E}_j^{\mathrm{inc}}$ is the incident electric field, which is given by $\mathbf{E}_j^{\mathrm{inc}} = \mathbf{E}_0 exp(ik \cdot \mathbf{r}_j - i\omega t)$. $\mathbf{E}_0$ is the amplitude of the electric field intensity and k can be expressed as ω/c. $\mathbf{A}_{jk}$ stands for the interaction matrix, where j and k are the number of dipoles. $\mathbf{A}_{jk}\mathbf{P}_k$ is the electric field at position $\mathbf{r}_j$, which is triggered by the dipole at position $\mathbf{r}_k$. It is given as [29]:

$$\mathbf{A}_{jk}\mathbf{P}_k = \frac{\exp(ik\mathbf{r}_{jk})}{\mathbf{r}_{jk}^3} \left\{ k^2 \mathbf{r}_{jk} \times (\mathbf{r}_{jk} \times \mathbf{P}_k) + \frac{(1 - ik\mathbf{r}_{jk})}{\mathbf{r}_{jk}^2} \times [\mathbf{r}_{jk}^2 \mathbf{P}_k - 3\mathbf{r}_{jk} \cdot \mathbf{P}_k] \right\}, \quad j \neq k \tag{2}$$

Biomedical Optics EXPRESS

If $\mathbf{A}_{jj}$ is defined as $\mathbf{A}_{jj} = -\alpha_j^{-1}$, then the scattering problem can be described as a set of linear equations as follows:

$$\sum_{k=1}^{N} \mathbf{A}_{jk}\mathbf{P}_k = \mathbf{E}_j^{\text{inc}} \tag{3}$$

The extinction, absorption, and scattering cross section can be calculated by:

$$C_{\text{ext}} = \frac{4\pi k}{|\mathbf{E}_0|^2} \sum_{j=1}^{N} \text{Im}(\mathbf{E}_j^{\text{inc},*} \cdot \mathbf{P}_j) \tag{4}$$

$$C_{\text{abs}} = \frac{4\pi k}{|\mathbf{E}_0|^2} \sum_{j=1}^{N} \left[\text{Im}(\mathbf{P}_j \cdot \alpha_j^{-1} \cdot \mathbf{P}_j^*) - \frac{2}{3}k^3|\mathbf{P}_j|^2\right] \tag{5}$$

$$C_{\text{sca}} = C_{\text{ext}} - C_{\text{abs}} \tag{6}$$

where $\mathbf{P}^*$ is the polarization of each dipole. The corresponding extinction, absorption, and scattering efficiency is the ratio of the cross section and πR_{eff}^2, where R_{eff} is the effective radius. R_{eff} is invariably utilized to characterize the size of an arbitrarily shaped small particle, which can be expressed as $R_{\text{eff}} = (3\,V/4\pi)^{1/3}$, where V is the volume of the particle. Then, the corresponding absorption (Q_{abs}), scattering (Q_{sca}), and extinction (Q_{ext}) efficiencies can be expressed as $Q_{\text{abs}} = C_{\text{abs}}/(\pi {R_{\text{eff}}}^2)$, $Q_{\text{sca}} = C_{\text{abs}}/(\pi {R_{\text{eff}}}^2)$, and $Q_{\text{ext}} = C_{\text{abs}}/(\pi {R_{\text{eff}}}^2)$, respectively. The detailed description of DDA can be found elsewhere [29–31].

The light propagation in biological tissue is calculated by the Monte Carlo method (MCM), which is widely applied [1,32,33]. The basic principle of the MCM is shown in Fig. 1. The details will not be repeated here and can be found in other studies [32–34]. It should be noted that the anisotropic scattering characteristic of both nanoparticles and tissues is taken into consideration in the present work. Therefore, before deciding the scattering direction of light during the execution of the MCM, it should be judged first that whether the light is interacting with tissue or nanoparticle. In the present work, this is achieved by generating a random number N_{rand}. If $N_{\text{rand}} > \beta_{\text{n}}/(\beta_{\text{n}} + \beta_{\text{t}})$, the light is interacting with tissue, where β_{n} and β_{t} are the attenuation coefficients of nanoparticle system and tissue, respectively. Otherwise, the light is interacting with nanoparticles. Afterwards, the scattering directions can be decided accordingly by the following equation if Henyey-Greenstein function (H-G) is applied [34]:

$$\cos\theta = \frac{1}{2g}\left[1 + g^2 - \left(\frac{1 - g^2}{1 - g + 2gN_{\text{rand}}}\right)\right] \tag{7}$$

where g is the asymmetry factor of tissue matrix or nanoparticles. In the present work, a three-parameter analytic phase function based on H-G phase function is also applied. The details can be found in the supporting information.

The Pennes bioheat transfer equation with light induced volumetric heat source Q_{r} is applied to solve the heat transfer problem in nanoparticle-embedded biological tissue [1]:

$$\rho c_{\text{p}} \frac{\partial T}{\partial t} = k\nabla^2 T + Q_{\text{b}} + Q_{\text{m}} + Q_{\text{r}} \tag{8}$$

where ρ, c_{p}, T, and k denote the density, specific heat, temperature, and thermal conductivity of the tissue, respectively. Q_{b} and Q_{m} stand for the heat transfer from the blood and the volumetric metabolic heat generation rate, respectively, where Q_{b} can be expressed as [35]:

$$Q_{\text{b}} = w_{\text{b}}\rho_{\text{b}}c_{\text{pb}}(T_{\text{b}} - T) \tag{9}$$

where w is the blood perfusion rate of the tissue. The subscript 'b' denotes blood.

Biomedical Optics EXPRESS

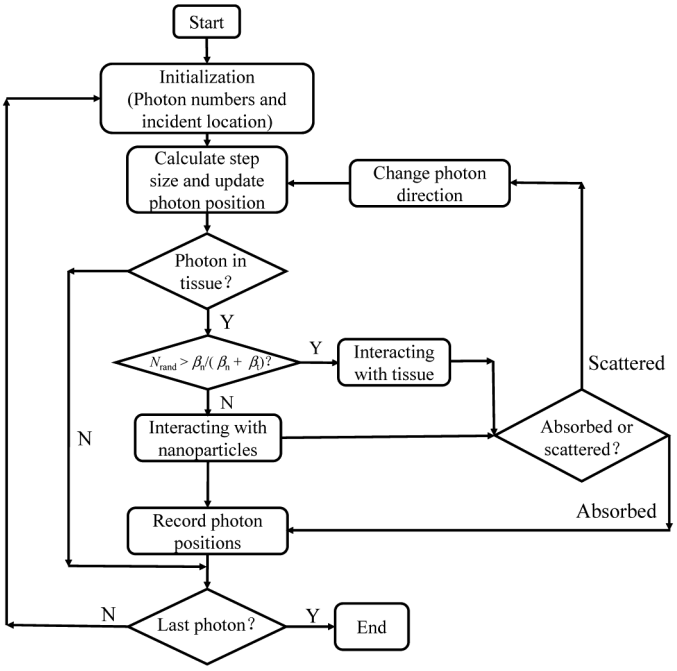

Fig. 1. Flowchart of Monte Carlo method.

3. Results and discussion

3.1. Non-uniform temperature distribution of laser-irradiated nanofluid

A very important issue that limits the development of laser induced thermal therapy is the non-uniform temperature distribution in the cancerous area, which may lead to inadequate treatment of tumors or overheating of the surrounding healthy tissue. This is decided by the propagation nature of light in semi-transparent media, which means that the energy carried by light attenuates while it travels through the medium. The attenuated energy can be divided into two parts which are either absorbed or scattered by the medium. Most of the previous studies are focused on solving this problem by manipulating the first part, which is usually realized by adding nanoparticles into the cancerous tissue to increase the absorption of the tumor, and therefore to distinguish cancerous tissue from healthy tissue. However, this approach is not sufficient since it may cause non-uniform temperature distribution inside the tumor, since the penetration depth of light in nanoparticle-embedded tissue can be very limited.

Fig. 2 shows the temperature distribution of nanofluid under the illumination of a 532 nm CW laser. It can be seen that the high temperature zone is located in the nanofluid side, near the air-fluid interface. In the photothermal therapy case, it will appear around the interface between cancerous and healthy tissue. The reason is that light attenuates rapidly after it reaches the nanofluid. Therefore, the expansion of the high temperature zone is driven by the light induced heat source and heat diffusion. During photothermal therapy, to avoid unwanted damage to surrounding healthy tissue, the effect of heat diffusion must be minimized. To gain deep insight into the light and heat transfer problems involved, a light and heat transfer model considering the anisotropic scattering of nanoparticles is established. Fig. 2(d) shows the temperature distribution along the center line of the cuvette surface. g represents the asymmetry factor in H-G scattering phase function. $g = 0.9$ and -0.9 denote forward and backward scattering, respectively. When g is set as 0.336, the scattering characteristic is very similar to that of a gold nanoparticle with

Biomedical Optics EXPRESS

radius $r = 80$ nm (see Fig. S1 in the Supporting Information). It can be seen from the numerical results that for the nanoparticles with backward scattering ($g < 0$), the temperature homogeneity is worse than those with forward scattering ($g > 0$), which means that by adjusting the scattering characteristic of the embedded nanoparticles, the temperature homogeneity can be improved. It is worth noting that the temperature homogeneity of the experimental results is worse than that of the numerical ones. It may be induced by the slight aggregation of nanoparticles [see Fig. 2(f)], which may increase the extinction coefficient of the nanofluid, and therefore reduce the penetration depth of light. However, this still needs to be further investigated for specific condition.

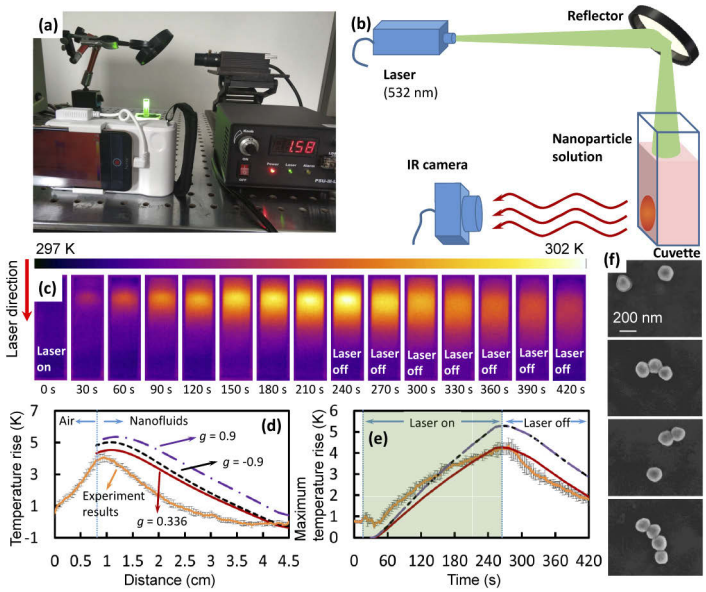

Fig. 2. Temperature change of nanofluid under the illumination of 532 nm CW laser. (a) Experimental setups; (b) schematic diagram of experimental system; (c) Measured temperature distribution of the cuvette surface using infrared camera with laser illuminated for 240 s; (d) Comparison of simulation (g = -0.9, 0.336, and 0.9) and experimental results of temperature change in the center line of the cuvette surface, where g represents the asymmetry factor of the H-G phase function. The initial temperature is considered as 298 K; (e) Maximum temperature rise as a function of time; (f) SEM images of nanofluid with nanoparticles of radius $r = 80$ nm.

3.2. *Anisotropic scattering of plasmonic nanoparticles*

To manipulate the scattering characteristic of nanoparticles, one must first know how the factors (shape, size, and material) affect the scattering directivity of nanoparticles. In this section, the anisotropic scattering of plasmonic nanoparticles is investigated. In the following content, the refractive index of the matrix media (water) is set as 1.33, which is frequently used in other references [2,11,36]. The aspect ratio (AR) of nanorods is defined as the ratio of cylinder length, not including end-caps, and cylinder dimeter. Regarding the triangular prism, AR is defined as the ratio of sides of the triangular cross section and the length of the prism.

It can be easily predicted that the radiation pattern of non-spherical nanoparticles will exhibit severe anisotropism. Here, the radiation patterns of a gold triangular nanoprism and nanorod with different incident directions of light are shown as an example (see Fig. 3). It can be seen that scattering phase function can be extremely anisotropic depending on the orientations of

Biomedical Optics EXPRESS

the nanoparticles, especially for triangular nanoprisms. Moreover, for nanorods, totally forward scattering and isotropic scattering can be achieved in certain conditions. It is worth mentioning that in biological tissues, the nanoparticles are distributed and oriented randomly. Therefore, to calculate the light scattering in biological tissues, the scattering phase function of non-spherical nanoparticles should be averaged by the results of several different orientations (see Fig. S4). Moreover, the number of the orientations considered should be selected carefully to obtain a sufficiently accurate solution, while at the same time it should be kept to a minimum to reduce computational costs. Here, we studied scattering properties of six different types of nanoparticles, spherical and non-spherical, including nanospheres, triangular nanoprisms, nanocubes, nanorods, and nanoshells ($Au@SiO_2$ and $SiO_2@Au$), aiming to develop a better solution for a more reasonable light delivery system in biological tissues. Fig. 4 illustrates the radiation patterns for the above-mentioned types of nanoparticles in different sizes averaged from 20×20 orientations irradiated by 532 nm and 808 nm lasers. It should be noted that 532 nm is selected specifically to illustrate the forward scattering properties, since forward scattering is more likely to appear under high frequency wave illumination. However, for thermal therapy, the wavelength located in the near-infrared region, such as 808 nm, is favorable for larger tissue penetration depth. It is very interesting to note that by averaging the directional scattering intensities, the radiation patterns for different shapes of nanoparticles seem to exhibit similar shapes, except for nanorods. However, the radiation patterns can all be described by the three-parameter analytic phase function (see Figs. S2 and S3), which can be attributed to that obtained by averaging the scattering intensities of different incident directions, and the non-spherical particles can be equivalent to spherical particles with an equivalent radius.

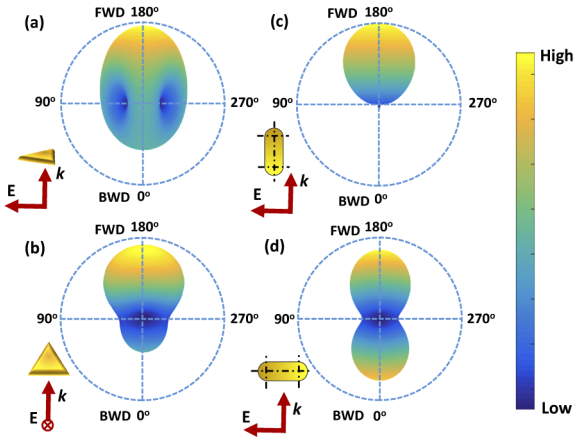

Fig. 3. Radiation patterns for (a-b) triangular nanoprism and (c-d) nanorod when laser is irradiated from different directions. The effective radius of nanoparticles is 50 nm. The incident wavelength is 532 nm. The aspect ratio of triangular nanoprism and nanorod are 2.0 and 3.0, respectively. FWD and BWD stand for forward and backward direction, respectively.

It also can be seen that the radiation pattern seems to also be related to the particle size. Taking the triangular nanoprism as an example, with decreasing particle radius, the radiation pattern turns from forward scattering to nearly isotropic scattering [see Fig. 4(b)]. Moreover, the incident wavelength is also an important factor that needs to be considered, which is of great importance for the scattering properties of nanoparticles. Fig. 5 illustrates the radiation patterns of gold nanospheres and $Au@SiO_2$ nanoshells as the function of wavelength. It is obvious that with increasing wavelength the radiation pattern of nanospheres goes from forward scattering to backward scattering, which is consistent with the conclusion for larger particles [37]. Interestingly, for nanoshells, two scattering peaks and one dip in the spectral scattering

Biomedical Optics EXPRESS

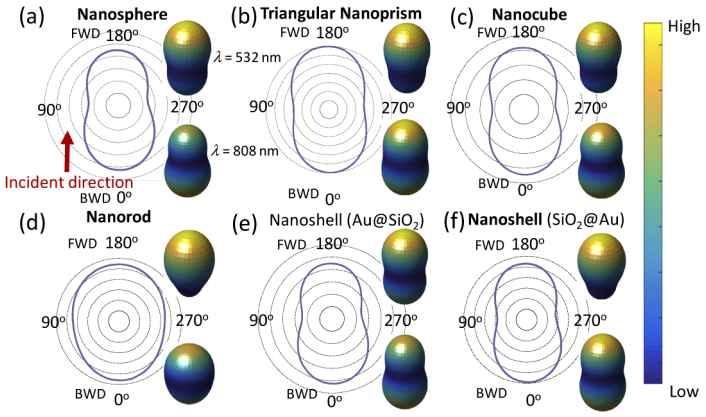

Fig. 4. Radiation patterns for (a) nanosphere; (b) triangular nanoprism; (c) nanocube; (d) nanorod; (e) nanoshell (Au@SiO_2); and (f) nanoshell (SiO_2@Au). The effective radius of the nanoparticles is set as 50 nm for the 2D radiation patterns with incident wavelength $\lambda = 808$ nm. The insets are 3D radiation patterns for corresponding nanoparticles for $\lambda = 532$ nm (upper) and $\lambda = 808$ nm (lower). The aspect ratio of triangular nanoprism and nanorod are 2.0 and 3.0, respectively. For nanoshell, the ratio of inner and outer diameters are 4 : 5.

curve exist. From the radiation patterns corresponding to the peaks and dip, it can be seen that this conclusion is also valid.

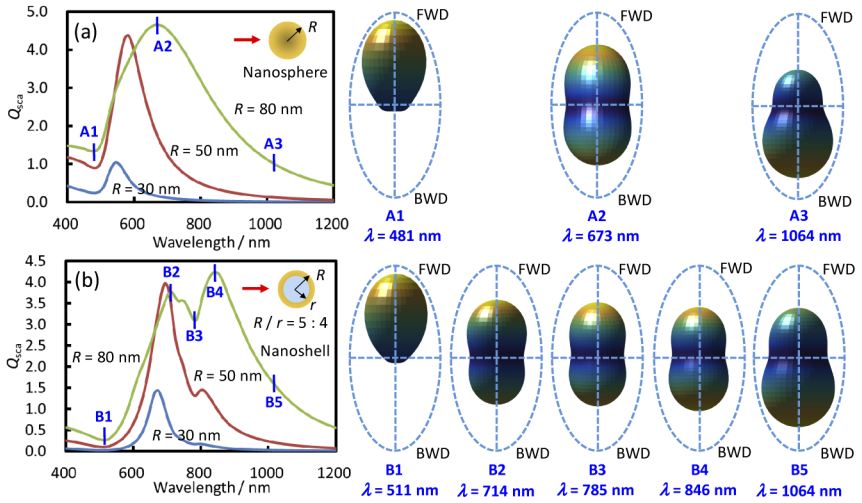

Fig. 5. Wavelength dependence of radiation patterns for (a) gold nanosphere and (b) gold nanoshell (Au@SiO_2). For nanoshell, the ratio of inner and outer diameters are 4 : 5.

From the above analysis, I can be concluded that the desired scattering characteristic can be obtained by tuning the incident wavelength or particles sizes. However, the laser wavelength applied in thermal therapy is usually limited to the "optical window". As can be seen from Fig. 5, the boundary for both backward scattering dominating and forward scattering dominating is the scattering peak, which means that when the incident wavelength is shorter than the wavelength corresponding to the scattering peak the nanoparticle will exhibit a forward-scattering characteristic. This is also valid for nanoparticles of other materials (see Fig. S7). Fortunately,

Biomedical Optics EXPRESS

the scattering peak can be tuned continuously in the near-infrared range [38], which means that the desired scattering patterns can be achieved by changing the size, shape, and component of nanoparticles without altering the applied laser wavelength. It should be noted that this conclusion is also consistent with previous investigations that Rayleigh scattering occurs in all directions when the particle size is much smaller than the light wavelength. However, when the particle size is comparable to the light wavelength (Mie scattering regime), incident light is predominantly scattered in the forward direction [37,39]. Therefore, from the point view of light propagation, it is suggested to use a kind of nanoparticle with larger radius or short wavelength laser during photothermal therapy. Meanwhile, despite the scattering properties, the light-to-heat conversion efficiency ($Q_{abs}/(Q_{abs}+Q_{sca})$) of nanoparticles should also be taken into consideration. It should be noticed that the peak of the absorption and scattering profiles do not always match (see Fig. 6). Even if they match, the photothermal conversion efficiency is always strongly related to wavelength. More importantly, under some circumstances, absorption dominates ($Q_{abs}/Q_{sca} > 1$) and sometimes scattering dominates ($Q_{abs}/Q_{sca} < 1$). This has a crucial influence on the SAR in biological tissues when irradiated by laser. However, in former studies, the wavelength close to the corresponding absorption peak is always the first choice, which may be not the optimal one since the SAR distribution is an important factor in LITT [1].

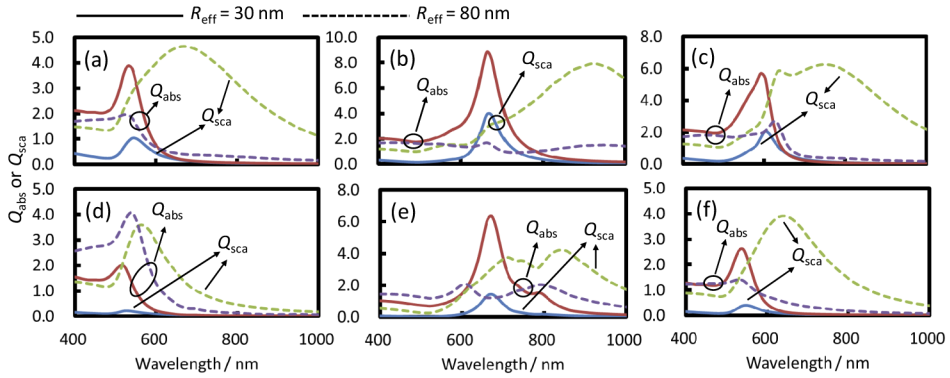

Fig. 6. Absorption and scattering efficiency for gold nanoparticles: (a) nanosphere; (b) triangular nanoprism; (c) nanocube; (d) nanorod; (e) nanoshell ($Au@SiO_2$); (f) Nanoshell ($SiO_2@Au$) with different effective radius. The aspect ratio of triangular nanoprism and nanorod are 2.0 and 3.0, respectively. For nanoshell, the ratio of inner and outer diameters are 4 : 5.

3.3. *Temperature increase analysis of tissue embedded with anisotropic scattering nanoparticles*

In this section, the inhomogeneity of temperature distribution in biological tissue embedded with nanoparticles during LITT is investigated. An efficient and practical way to control the temperature distribution in biological tissues is to manipulate the heat source distribution induced by laser irradiation, since the heat conduction process in tissues is very difficult, if not impossible, to control. The most favorable heat source distribution would be that the heat source induced by laser is totally concentrated in the tumorous zone, which enables heating of the tumor zone to hyperthermia conditions in a very short time without influencing the nearby healthy tissue. However, due to the scattering and absorption effects, the light penetration depth in tissues is very limited even for the wavelength within the near-infrared window, which will be further reduced with the injection of nanoparticles. This means that when irradiated by laser the superficial tissue or the interface between the tumor and biological tissue will be heated first without heating the inner part of tumor. Therefore, to improve the penetration depth of light in tumors will reduce the

Biomedical Optics EXPRESS

overheating of nearby healthy tissue. Obviously, the asymmetry factor g of biological tissue will greatly affect light propagation and heat generation in tissues (see Fig. 7). The optical properties of tissues were obtained from Ref. [33] and the input parameters are listed in Table 1. It can be seen that for backward scattering, most of the incident light is absorbed by the superficial tissue. The SAR distribution is highly heterogeneous, which may lead to the damage of healthy tissue. However, for the forward-scattering tissue, SAR distribution is nearly uniform, which means uniform heating of the tumor.

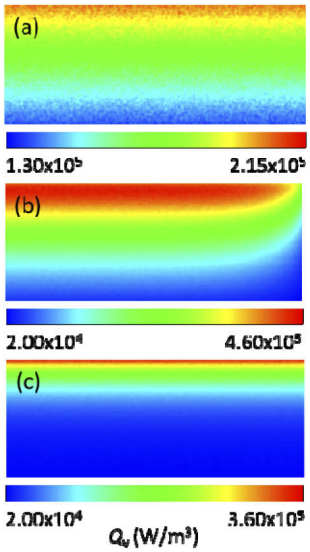

Fig. 7. Heat generation rate in a 2D biological tissue without nanoparticles embedded: (a), (b), and (c) show the heat generation rate distributions of biological tissue without nanoparticles for forward scattering ($g = 1.0$), isotropic scattering ($g = 0$), and backward scattering ($g = -1.0$), respectively. The upper boundary of the physical model is exposed to laser irradiation. The left boundary of the biological tissue is set as symmetrical. Other boundaries are set as transparent.

Table 1. Physical parameters in optical transfer model.

	Parameters	Value
Optical properties of tissue	Absorption coefficient	41 m^{-1}
	Scattering coefficient	500 m^{-1}
	Absorption coefficient (with nanospheres $R = 50$ nm)	116 m^{-1}
	Scattering coefficient (with nanospheres $R = 50$ nm)	708 m^{-1}
Properties of gold nanoparticles	Absorption efficiency	0.167
	Scattering efficiency	0.462
	Volume fraction	3.0×10^{-5}
Other properties	Laser intensity	5000 W/m^2
	Heating time	50 s
	Length	0.025 m
	Height	0.01 m
	Grid number	100×250
	Number of photons in each grid	10^6

Biomedical Optics EXPRESS

Unfortunately, to the best of our knowledge, manipulating the asymmetry factor of tissue is very difficult to achieve, if it is possible at all. However, the asymmetry factor of the injected nanoparticles can be easily tuned according to the above analysis. Thus, the influence of the asymmetry factor of nanoparticles on the light and heat transportation in laser-irradiated tissues was studied. The nanoparticles are assumed to be uniformly distributed in the tumorous area. To simplify the problem under consideration, the asymmetry factors of nanoparticles are approximately set as 1.0, 0, and -1.0, corresponding to forward, isotropic, and backward scattering, respectively. Moreover, the actual g value of the asymmetry factor of gold nanospheres with a radius 50 nm was also considered. It should be notice that the scattering pattern of nanosphere with $R = 50$ cannot be described using the traditional H-G function. It should be fitted using a three-parameter function, which is introduced in the Supporting Information. It is found that, even when keeping the asymmetry factor of the tissue constant, the scattering pattern of a nanoparticle alone can contribute substantially to the light propagation pattern in tissue (see Fig. 8). To be specific, forward-scattering nanoparticles are favorable for a more uniform distribution of the heat source. It is worth noting that when the asymmetry factor of the tissue matrix is set as 0.9, the influence of the asymmetry factor of nanoparticles is weakened, but is still noticeable. Moreover, when the asymmetry factor of nanoparticles is set as an actual gold nanosphere with $R = 50$ nm instead of being treated as isotropic scattering, the distribution of the heat generation rate is almost the same. This is because the radiation pattern of $R = 50$ nm nanoparticles at 808 nm is almost isotropic. However, as mentioned above, this can be tuned by selecting the nanoparticle size and shape or the applied laser wavelength.

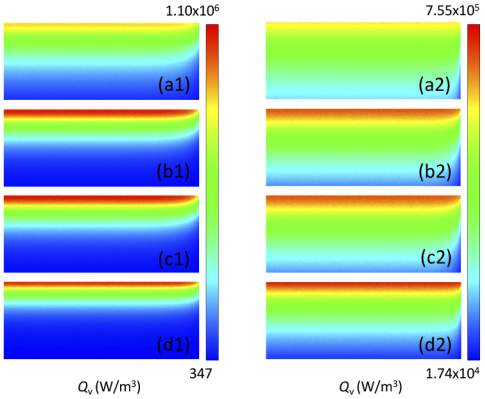

Fig. 8. Heat generation rate in a 2D biological tissue with nanoparticles embedded: (a1) and (a2) forward scattering ($g = 1.0$); (b1) and (b2) actual scattering properties of gold nanosphere with $R = 50$ nm under 808 nm laser irradiation; (c1) and (c2) isotropic scattering ($g = 0$); and (d1) and (d2) backward scattering ($g = -1.0$). In (a1)-(d1), the asymmetry factor of tissue are set as 0, which means isotropic scattering. In (a2)-(d2), the asymmetry factor of tissue are set as 0.9, corresponding to forward scattering.

To examine the contribution of non-uniform distribution of the heat generation rate on the temperature distribution, the heat transfer problem of tissue under laser irradiation was investigated. Fig. 9 shows the physical model and boundary conditions of the bio-heat transfer problem under consideration. The tissue surface is assumed to be irradiated by laser vertically. The temperature distributions of biological tissue with tumor embedded with nanoparticles for different scattering patterns are illustrated in Fig. 10. The solid line is the boundary of a heating area. $\Delta T < 10$ K means that the temperature difference (the highest temperature minus the lowest temperature in the marked region) is less than 10 K, which is used as an indicator to show the temperature uniformity in the present work. It can be seen that for the forward

Biomedical Optics EXPRESS

scattering, the temperature distribution inside tumor has the best uniformity, when the asymmetry factor of tissue matrix is set as 0.9. Furthermore, it can be seen that the results of practical nanoparticle are similar to those of the isotropic scattering cases in the present situation. However, it should be known that the asymmetry factor of actual nanoparticles can be further improved by tuning the size, shape, or component of the nanoparticle. The normalized temperature of the left-hand boundary is shown in Fig. 11, in which the normalized temperature means that the temperature along the left-hand boundary for different cases is divided by the highest temperature corresponding to that situation. It can be seen more clearly that with the asymmetry factor g of nanoparticles changing from backward to forward scattering, the temperature distribution inside the tumorous area will become more uniform. Similar results can be obtained for biological

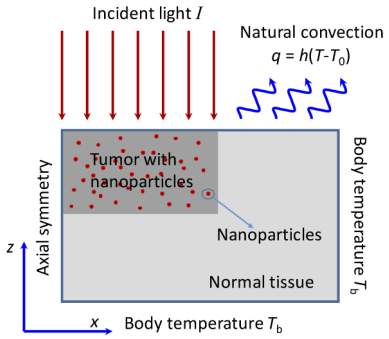

Fig. 9. Physical model and boundary conditions of bio-heat transfer.

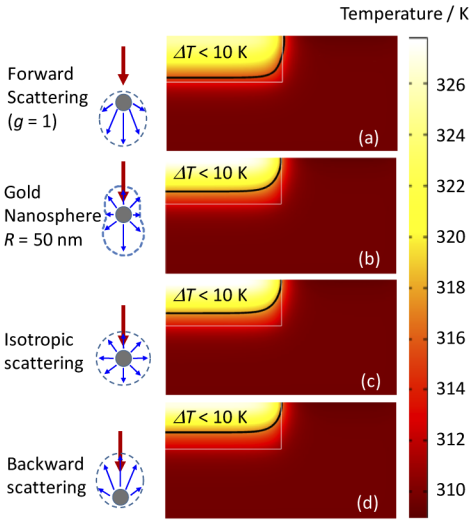

Fig. 10. Temperature distribution of biological tissue with tumor embedded with nanoparticles when irradiated by laser for 50 s: (a) forward scattering (g = 1.0); (b) actual scattering properties of gold nanosphere with R = 50 nm under 808 nm laser irradiation; (c) isotropic scattering (g = 0); and (d) backward scattering (g = -1.0) nanoparticles, respectively. The asymmetry factor of tissue is set as 0.9. The nanoparticles are assumed to be distribution uniformly and oriented randomly inside tumor. Other optical properties and conditions are the same as Fig. 8. The white lines are the boundaries of tumor and the black lines separate the region that with temperature difference less than 10 K compared to the highest temperature in the tissue surface.

Biomedical Optics EXPRESS

tissue embedded with gold nanorods (see Figs. S10 and S11). Therefore, it can be concluded that by carefully selecting the asymmetry factor of the embedded nanoparticles, the temperature uniformity can be improved in tumor during laser induced thermal therapy.

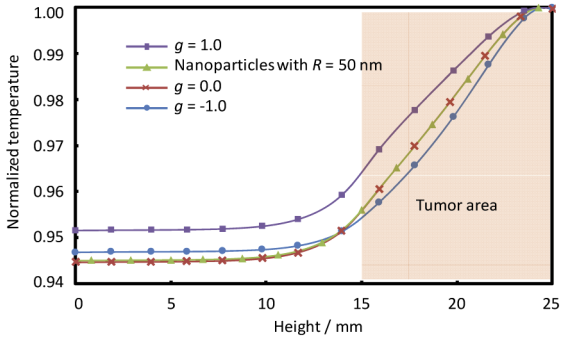

Fig. 11. Normalized temperature along the left boundary of biological tissue with tumor with nanoparticles.

4. Conclusions

In the present work, the influence of anisotropic scattering of nanoparticles on the uniformity of SAR distribution in tumors during LITT is investigated, aiming to increase the temperature uniformity insider tumors. The anisotropic scattering properties of different nanoparticles are also explored. On this basis, the SAR and temperature distributions of biological tissue embedded with nanospheres and nanorods for different scattering patterns during laser irradiation are presented. It was found that the anisotropic scattering characteristics of nanoparticle are strongly dependent on its shape, size, orientation, and the incident wavelength. To obtain a better outcome from photothermal therapy, the scattering properties of nanoparticles are also very important factors that need to be taken into consideration along with the absorption efficiency. Further investigation found that nanoparticles that predominantly scatter in the forward direction are beneficial to the forward propagation of light, which can improve the uniformity of SAR and temperature distributions. In conclusion, the anisotropic scattering properties of nanoparticles should also be considered when selecting nanoparticles as thermal contrast agents. To be specific, from the aspect of light propagation, it is suggested that larger nanoparticles or short wavelength laser should be applied in the application of photothermal therapy to obtain a more uniform temperature distribution in the tumorous area. In the meantime, it should be noted that it is a very complicate problem for the selecting of nanoparticles in clinical applications. There are also many other factors that need to be taken into consideration, such as the deliver and uptake of nanoparticles in biological system. A comprehensive future work is also need to show the outcome of nanoparticles selection under this guideline.

Funding. National Natural Science Foundation of China (51806047); China Postdoctoral Science Foundation (2019T120264); Heilongjiang Provincial Postdoctoral Science Foundation (LBH-Z18094); Natural Science Foundation of Heilongjiang Province (LH2019E047); H2020 Marie Skłodowska-Curie Actions (839641).

Acknowledgments. A very special acknowledgement is made to B.T. Draine (Princeton University) and P. J. Flatau (University of California) for their DDA code, DDSCAT 7.3.

Disclosures. The authors declare no conflicts of interest

Supplemental document. See Supplement 1 for supporting content.

References

1. Y. Ren, H. Qi, Q. Chen, and L. Ruan, "Thermal dosage investigation for optimal temperature distribution in gold nanoparticle enhanced photothermal therapy," Int. J. Heat Mass Transfer **106**, 212–221 (2017).

Biomedical Optics EXPRESS

2. B. Geng, D. Yang, D. Pan, L. Wang, F. Zheng, W. Shen, C. Zhang, and X. Li, "Nir-responsive carbon dots for efficient photothermal cancer therapy at low power densities," Carbon **134**, 153–162 (2018).
3. S. Yang, Z. Li, Y. Wang, X. Fan, Z. Miao, Y. Hu, Z. Li, Y. Sun, F. Besenbacher, and M. Yu, "Multifunctional bi@ppy-peg core-shell nanohybrids for dual-modal imaging and photothermal therapy," ACS Appl. Mater. Interfaces **10**(2), 1605–1615 (2018).
4. V. N. Tran, V. G. Truong, Y. W. Lee, and H. W. Kang, "Effect of optical energy modulation on the thermal response of biological tissue: Computational and experimental validations," Biomed. Opt. Express **11**(12), 6905–6919 (2020).
5. V. Siahpoush, S. Ahmadi-kandjani, and A. Nikniazi, "Effect of plasmonic coupling on photothermal behavior of random nanoparticles," Opt. Commun. **420**, 52–58 (2018).
6. N. S. Abadeer and C. J. Murphy, "Recent progress in cancer thermal therapy using gold nanoparticles," J. Phys. Chem. C **120**(9), 4691–4716 (2016).
7. L. Yan, J. Zeng, Y. Jiang, X. Zhen, T. Wang, S. Qiu, X. Lou, M. Gao, and K. Pu, "Enhancing both biodegradability and efficacy of semiconducting polymer nanoparticles for photoacoustic imaging and photothermal therapy," ACS Nano **12**(2), 1801–1810 (2018).
8. Y. Ren, Q. Chen, H. Qi, and L. Ruan, "Experimental comparison of photothermal conversion efficiency of gold nanotriangle and nanorod in laser iinduced thermal therapy," Nanomaterials **7**(9), 238 (2017).
9. A. B. Bucharskaya, G. N. Maslyakova, M. L. Chekhonatskaya, G. S. Terentyuk, N. A. Navolokin, B. N. Khlebtsov, N. G. Khlebtsov, A. N. Bashkatov, E. A. Genina, and V. V. Tuchin, "Plasmonic photothermal therapy: Approaches to advanced strategy," Lasers Surg. Med. **50**, 1025–1033 (2018).
10. L. A. Dombrovsky, V. Timchenko, and M. Jackson, "Indirect heating strategy for laser induced hyperthermia: An advanced thermal model," Int. J. Heat Mass Transfer **55**(17-18), 4688–4700 (2012).
11. L. A. Dombrovsky, V. Timchenko, M. Jackson, and G. H. Yeoh, "A combined transient thermal model for laser hyperthermia of tumors with embedded gold nanoshells," Int. J. Heat Mass Transfer **54**(25-26), 5459–5469 (2011).
12. N. K. Simón M, JT Jørgensen, LB Oddershede, and A Kjaer, "Fractionated photothermal therapy in a murine tumor model: Comparison with single dose," Int. J. Nanomed. **14**, 5369–5379 (2019).
13. M. Alrahili, V. Savchuk, K. McNear, and A. Pinchuk, "Absorption cross section of gold nanoparticles based on nir laser heating and thermodynamic calculations," Sci. Rep. **10**, 18790 (2020).
14. N. Katchinskiy, R. Godbout, and A. Y. Elezzabi, "Evidence of femtosecond-laser pulse induced cell membrane nanosurgery," Proc. SPIE **10062**, 1006203 (2017).
15. E. V. P. Komarala, H. Tyagi, S. Thiyagarajan, L. Pradhan, M. Aslam, and D. Bahadur, "Nir absorbing au nanoparticle decorated layered double hydroxide nanohybrids for photothermal therapy and fluorescence imaging of cancer cells," J. Mater. Chem. B **5**(21), 3852–3861 (2017).
16. M. A. Behnam, F. Emami, Z. Sobhani, O. Koohihosseinabadi, A. R. Dehghanian, S. M. Zebarjad, M. H. Moghim, and A. Oryan, "Novel combination of silver nanoparticles and carbon nanotubes for plasmonic photo thermal therapy in melanoma cancer model," Adv. Pharm. Bull. **8**(1), 49–55 (2018).
17. H. Norouzi, K. Khoshgard, and F. Akbarzadeh, "In vitro outlook of gold nanoparticles in photo-thermal therapy: A literature review," Laser Med. Sci. **33**(4), 917–926 (2018).
18. A. E. Krasnok, A. E. Miroshnichenko, P. A. Belov, and Y. S. Kivshar, "All-dielectric optical nanoantennas," Opt. Express **20**(18), 20599–20604 (2012).
19. V. E. Babicheva and A. B. Evlyukhin, "Resonant suppression of light transmission in high-refractive-index nanoparticle metasurfaces," Opt. Lett. **43**(21), 5186–5189 (2018).
20. N. O. Lank, P. Johansson, and M. Kall, "Directional scattering and multipolar contributions to optical forces on silicon nanoparticles in focused laser beams," Opt. Express **26**(22), 29074–29085 (2018).
21. P. D. Terekhov, K. V. Baryshnikova, Y. A. Artemyev, A. Karabchevsky, A. S. Shalin, and A. B. Evlyukhin, "Multipolar response of nonspherical silicon nanoparticles in the visible and near-infrared spectral ranges," Phys. Rev. B **96**(3), 035443 (2017).
22. A. Krasnok, S. Li, S. Lepeshov, R. Savelev, D. G. Baranov, and A. Alú, "All-optical switching and unidirectional plasmon launching with nonlinear dielectric nanoantennas," Phys. Rev. Appl. **9**(1), 014015 (2018).
23. S. Jiang, M. J. Digonnet, A. B. Evlyukhin, A. S. Shalin, A. Karabchevsky, Y. A. Artemyev, K. V. Baryshnikova, and P. D. Terekhov, "Optical multipole resonances of non-spherical silicon nanoparticles and the influence of illumination direction," Proc. SPIE **10528**, 1052802 (2018).
24. C. Tao, L. An, J. Lin, Q. Tian, and S. Yang, "Surface plasmon resonance–enhanced photoacoustic imaging and photothermal therapy of endogenous h2s-triggered au@cu2o," Small **15**, 1903473 (2019).
25. Y. Yin, Y. Ren, H. Li, and H. Qi, "Characteristic analysis of light and heat transfer in photothermal therapy using multiple-light-source heating strategy," Int. J. Therm. Sci. **158**, 106533 (2020).
26. S. Soni, H. Tyagi, R. A. Taylor, and A. Kumar, "Investigation on nanoparticle distribution for thermal ablation of a tumour subjected to nanoparticle assisted thermal therapy," J. Therm. Biol. **43**, 70–80 (2014).
27. S. Soni, H. Tyagi, R. A. Taylor, and A. Kumar, "Role of optical coefficients and healthy tissue-sparing characteristics in gold nanorod-assisted thermal therapy," Int. J. Hyperther. **29**(1), 87–97 (2013).
28. K.-S. Lee and M. A. El-Sayed, "Dependence of the enhanced optical scattering efficiency relative to that of absorption for gold metal nanorods on aspect ratio, size, end-cap shape, and medium refractive index," J. Phys. Chem. B **109**(43), 20331–20338 (2005).

Biomedical Optics EXPRESS

29. B. T. Draine, "Discrete-dipole approximation and its application to interstellar graphite grains," Astrophys. J. **333**, 848–872 (1988).
30. Y. Ren, H. Qi, Q. Chen, S. Wang, and L. Ruan, "Localized surface plasmon resonance of nanotriangle dimers at different relative positions," J. Quant. Spectrosc. Radiat. Transfer **199**, 45–51 (2017).
31. B. T. Draine and P. J. Flatau, "Discrete-dipole approximation for scattering calculations," J. Opt. Soc. Am. A **11**(4), 1491–1499 (1994).
32. N. Manuchehrabadi and L. Zhu, "Development of a computational simulation tool to design a protocol for treating prostate tumours using transurethral laser photothermal therapy," Int. J. Hyperther. **30**(6), 349–361 (2014).
33. N. Manuchehrabadi, Y. Chen, A. Lebrun, R. Ma, and L. Zhu, "Computational simulation of temperature elevations in tumors using monte carlo method and comparison to experimental measurements in laser photothermal therapy," J. Biomech. Eng. Trans. ASME **135**(12), 121007 (2013).
34. S. A. Prahl, M. Keijzer, S. L. Jacques, and A. J. Welch, "A monte carlo model of light propagation in tissue," in *SPIE Proceedings of Dosimetry of Laser Radiation in Medicine and Biology* (SPIE, Berlin, Germany, 1989), pp. 102–111.
35. H. H. Pennes, "Analysis of tissue and arterial blood temperatures in the resting human forearm," J. Appl. Physiol. **1**(2), 93–122 (1948).
36. S. R. Panikkanvalappil, N. Hooshmand, and M. A. El-Sayed, "Intracellular assembly of nuclear-targeted gold nanosphere enables selective plasmonic photothermal therapy of cancer by shifting their absorption wavelength toward near-infrared region," Bioconjug. Chem. **28**(9), 2452–2460 (2017).
37. H. C. V. D. Hulst, *Light scattering by small particles* (Dover Publications, 1981).
38. P. K. Jain, K. S. Lee, I. H. El-Sayed, and M. A. El-Sayed, "Calculated absorption and scattering properties of gold nanoparticles of different size, shape, and composition: Applications in biological imaging and biomedicine," J. Phys. Chem. B **110**(14), 7238–7248 (2006).
39. H. Kim and J. H. Chang, "Increased light penetration due to ultrasound-induced air bubbles in optical scattering media," Sci. Rep. **7**(1), 16105 (2017).